Astronomy & Astrophysics manuscript no. 8263buat
March 5, 2008

© ESO 2008

arXiv:0803.0414v1 [astro-ph] 4 Mar 2008

Star formation history of galaxies from z=0 to z=0.7

A backward approach to the evolution of star-forming galaxies.

V. Buat[1], S. Boissier[1], D. Burgarella[1], T. T. Takeuchi[2], E. Le Floc'h[3], D. Marcillac[4], J. Huang[5], M. Nagashima[6], and M. Enoki[7]

[1] Observatoire Astronomique Marseille Provence, Laboratoire d'Astrophysique de Marseille, BP8, 133761 Marseille cedex 12, France
e-mail: `veronique.buat@oamp.fr`

[2] Institute for Advanced Research, Nagoya University, Furo-cho, Chikusa-ku, Nagoya 464-8601, Japan

[3] Spitzer fellow, Institute for Astronomy, University of Hawaii, 2680 Woodlawn Drive, Honolulu, HI 96822

[4] Steward Observatory, University of Arizona, 933 North Cherry Avenue, Tucson, AZ 85721, USA

[5] Harvard-Smithsonian Center for Astrophysics, 60 Garden Street, Cambridge, MA 02138

[6] Faculty of Education, Nagasaki University, Nagasaki 852-8521, Japan

[7] Faculty of Bussiness Administration, Tokyo Keizai University, 1-7-34, Minami-cho, Kokubunji, Tokyo, 185-8502, Japan

ABSTRACT

Aims. We investigate whether the mean star formation activity of star forming galaxies from z=0 to z=0.7 in the GOODS-S field can be reproduced by simple evolution models of these systems. In this case, such models might be used as first order references for studies at higher z to decipher when and to what extent a secular evolution is sufficient to explain the star formation history in galaxies.
Methods. We selected star-forming galaxies at z=0 and at z=0.7 in IR and in UV to have access to all the recent star formation. We focused on galaxies with a stellar mass ranging between 10^{10} and 10^{11} $M_\odot$ for which the results are not biased by the selections. We compared the data to chemical evolution models developed for spiral galaxies and originally built to reproduce the main characteristics of the Milky Way and nearby spirals without fine-tuning them for the present analysis.
Results. We find a shallow decrease in the specific star formation rate (SSFR) when the stellar mass increases. The evolution of the SSFR characterizing both UV and IR selected galaxies from z=0 to z=0.7 is consistent with the models built to reproduce the present spiral galaxies. There is no need to strongly modify of the physical conditions in galaxies to explain the average evolution of their star formation from z=0 to z=0.7. We use the models to predict the evolution of the star formation rate and the metallicity on a wider range of redshift and we compare these predictions with the results of semi-analytical models
Conclusions. .

Key words. galaxies: evolution-galaxies: stellar content-infrared: galaxies-ultraviolet: galaxies

1. Introduction

A lot of recent studies have explored the relation between the stellar mass and the star formation rate (SFR) in galaxies at different redshifts. It has been shown that star formation critically depends on galaxy mass both at low and high redshift (e.g. Gavazzi et al., 2002; Brinchmann et al., 2004; Feulner et al., 2005, and reference therein). The general process called "downsizing" (Cowie et al., 1996) is now commonly accepted: it can be summarized by an early and rapid formation of massive galaxies, whereas low-mass systems evolve more smoothly, being still actively forming stars at z=0. The galaxies are usually subdivided into active star-forming and quiescent systems within which star formation has been quenched. When only star-forming galaxies are concerned, the specific star formation rate (star formation rate divided by stellar mass) seems to exhibit a flatter distribution as a function of the stellar mass than when the whole population of galaxies is accounted for (e.g. Daddi et al., 2007; Elbaz et al., 2007; Iglesias-Páramo et al., 2007).

Physical processes that might be at the origin of or might influence the quenching of the star formation in massive galaxies have been extensively discussed (e.g. Dekel & Birnboim, 2006; Bundy et al., 2005, 2006, and references therein). Conversely there are only very few attempts to propose realistic star formation histories to explain the trends that are observed: most of the studies only explore very crude scenarios like a constant star formation rate or an instantaneous burst (Feulner et al., 2005). Recently, Noeske et al. (2007) have proposed a more sophisticated model with an exponential star formation history whose parameters are mass-dependent: less massive galaxies have a longer e-folding time and begin their formation more recently. Their model is based on two parameters: the e-folding time τ and

---

Send offprint requests to: V. Buat

redshift of galaxy formation z_f, which are fitted to their data. The redshift formation z_f is likely to be representative of the bulk of the star formation: a galaxy with a stellar mass of $\sim 10^{10}$M⊙ would form at $z_f = 1$ against $z_f = 3$ for more massive objects $\sim 10^{11}$M⊙.

In this paper, we follow a different approach. We start from a physical model built to reproduce the mean properties of local star-forming disk galaxies. We analyze how this model, without any modification or adjustment, can reproduce the evolution of the star formation observed with z. Practically speaking, we use a grid of models predicting the chemical and spectrophotometric evolution of spiral galaxies. These models were calibrated in the Milky Way (Boissier & Prantzos, 1999) and successfully reproduce the properties of nearby spiral galaxies (Boissier & Prantzos, 2000). The redshift formation z_f is taken to be equal to 6 for all the galaxies and represents the time when the first stars begin to form.

Our work is motivated by the recent findings that the UV and IR luminosity functions at intermediate redshifts (up to z $\sim 0.7-1$) are almost dominated by normal spiral or irregular galaxies (Bell et al., 2005; Wolf et al., 2005; Melbourne et al., 2005; Zheng et al., 2007b; Zamojski et al., 2007). The role of major mergers does not seem to govern the star formation at these redshifts, one can expect those galaxy evolution models that assume a smooth evolution to be appropriate for the interpretation of the observations.

In section 2 we describe the samples of sta-forming galaxies at z=0 and z=0.7 and the derivation of the main parameters useful to this study: the star formation rates (SFR) and stellar masses ($M_{\rm star}$). The selections are performed in rest-frame IR (60 or 15μm) and UV (1530Å) in order to be sure to pick up all star-forming galaxies at these redshifts. The characteristics of these selections are outlined in section 3. Specific star formation rates (SFRs divided by $M_{\rm star}$) are analyzed in section 4. The evolutionary models are presented in section 5 where we propose a simple analytical formulation for the SFR history of each galaxy. In section 6 the models are compared to the data. We also compare our results to more sophisticated (semi-analytical) models and give predictions for higher z. Section 7 is devoted to the conclusions.

Throughout this article, we use the cosmological parameters $H_0 = 70$ km s^{-1} Mpc^{-1}, $\Omega_M = 0.3$ and $\Omega_\lambda = 0.7$. All magnitudes are quoted in the AB system. The IR luminosity $L_{\rm IR}$ is defined over the wavelength range 8-1000 μm. The UV luminosity $L_{\rm UV}$ is defined as νL_ν. The luminosities are expressed in solar units with $L_\odot = 3.83\ 10^{33}$ergs^{-1}

2. Data sets, SFRs and stellar mass estimates

Our goal is to study the evolution of star-forming galaxies from the local universe to intermediate redshift ($z \leq\sim 1$) by comparing observations to the predictions of models of their evolution. Therefore we need to build galaxy samples that are representative of the overall star formation and we must avoid quiescent galaxies. The best way to focus on star-forming galaxies is to select them according to their SFR. Newly formed stars emit most of their light in the UV and a large fraction of their emission is re-processed in the IR via dust heating. Therefore we select the galaxy samples by using these two wavelength ranges: UV and IR.

We use local samples already built from GALEX and IRAS data at 1530 Å and 60 μm (Buat et al., 2007b). At intermediate z the deepest GALEX and SPITZER surveys can be used to build similar samples to z=0. Practically speaking, we work at z=0.7 to avoid K-corrections. At this redshift the GALEX near-ultraviolet band at 2310 Å corresponds to a 1530 Å rest frame, the UV wavelength at which galaxies have been selected at z=0 (far-ultraviolet band of GALEX). The SPITZER/MIPS observations at 24 μm correspond to $\sim$ 15 μm in the rest frame of galaxies at z=0.7. Although 15 μm does not directly correspond to the IRAS 60μm band, this mid-infrared wavelength range has been intensively studied, so we will be able to derive total infrared luminosities $L_{\rm IR}$ from these mono-wavelength data.

Rest-frame, near-infrared (NIR) data will be needed to estimate stellar masses, whereas the UV/IR selections ensure we can measure the current star formation: at z=0 they were estimated by Buat et al. (2007b) from 2MASS data. At z=0.7 the IRAC observations at 3.6 μm correspond to the K-band rest frame.
All the UV data are corrected for Galactic extinction using the Schlegel et al. (1998) maps and the Galactic extinction law of Cardelli et al. (1989). We have gathered the main characteristics of the samples described below in Table 1.

2.1. z=0 samples

Buat et al. (2007b) built two samples of galaxies selected at 60 μm (IR selected sample) and at 1530Å (UV selected sample) with a very high detection rate at 1530Å and 60 μm, respectively. A short description of the samples is made in Table 1. The original samples were flux-limited: the limiting luminosities reported in the table correspond to the faintest bins of the luminosity functions built with these samples (cf. Fig.3 of Buat et al., 2007b). Here we use the mean (volume-averaged) trends found from these samples. The SFRs are estimated by adding the star formation rate measured from the IR and the observed UV emissions as preconised by Iglesias-Páramo et al. (2006) assuming a constant SFR over 10^8 years. The only modification that we perform here is to use the initial mass function (IMF) of Kroupa (2001) since it is commonly used in recent studies and it is more consistent with the models used in this paper. From Starburst99 (Leitherer et al., 1999) we obtain:

$$\log(SFR_{\rm IR})_{\rm M_\odot\ yr^{-1}} = \log(L_{\rm IR})_{\rm L_\odot} - 9.97 \quad (1)$$

$$\log(SFR_{\rm UV})_{\rm M_\odot\ yr^{-1}} = \log(L_{\rm UV})_{L_\odot} - 9.69 \quad (2)$$

We follow Iglesias-Páramo et al. (2006) to estimate the total SFR:

$$SFR = (1-\eta)\cdot SFR_{\rm IR} + SFR_{\rm UV} \quad (3)$$

where η is the fraction of dust emission due to the heating by old stars and not related to the recent star formation. The introduction of this factor was found to be mandatory for making consistent star formation indicators (Bell, 2003; Hirashita et al., 2003; Iglesias-Páramo et al., 2004, 2006). Following Iglesias-Páramo et al. (2006) we take $\eta = 0.3$.

The stellar mass is calculated from H magnitudes as in Buat et al. (2007b). We use the Bell et al. (2003) $M/L_{\rm H}$ calibrations adopting a mean B-V color of 0.6 mag (Buat et al., 2007b) and a Kroupa et al. (1993) IMF. It corresponds to $M/L_{\rm H}$=0.58 in solar units. According to Bell et al. (2007), using a Kroupa (2001) IMF instead of a Kroupa et al. (1993) one would lead to similar stellar masses (within 10%). We have also checked (Buat et al., 2007b) that very similar masses would be obtained using K magnitudes instead of the H ones.

Table 1. Description of the samples. At z=0 all the characteristics come from Buat et al. (2007b), the limiting $L_{\rm IR}$ is estimated from the luminosity at 60 μm by applying a bolometric correction of 2.5 (Buat et al., 2007b). The samples at z=0.7 are fully described in section 2.2

	z=0	z=0.7
IR selection	IRAS $f_{60} > 0.6$Jy 665 galaxies $L_{\rm IR} \geq 2.5\,10^9 {\rm L}_\odot$	SPITZER/MIPS $f_{24} > 0.024$mJy 280 galaxies $L_{\rm IR} \geq 2.2\,10^{10} {\rm L}_\odot$
UV selection	GALEX FUV(1530Å) ≤ 17mag 656 galaxies $L_{\rm UV} \geq 3\,10^8 {\rm L}_\odot$	GALEX NUV(2310Å) ≤ 25.5mag 247 galaxies $L_{\rm UV} \geq 2.5\,10^9 {\rm L}_\odot$

2.2. z=0.7 samples

2.2.1. IR-selected sample

We start with the GOODS observations of the Chandra deep field south (CDFS) (Dickinson & Giavalisco, 2002). The source extraction and flux measurements were performed at 24 μm using DAOPHOT (Stetson, 1987) in a same way as in Le Floc'h et al. (2005). The detection limit at 3 σ is found to be 0.016 mJy. We have checked the completeness of our data by comparing the slope of the differential counts with models (Lagache et al., 2003; Takeuchi et al., 2001) and data obtained in the HDF-N (Chary et al., 2004). The data appear to be complete down to ~0.024 mJy. These values fully agree with those found by Elbaz et al. (2007) for the same set of data. We adopt a secure limit of 0.024 mJy to build our sample (Elbaz et al., 2007). Cross correlations with COMBO-17 (Wolf et al., 2004) were performed to get the redshift of the sources within a tolerance radius of 2" (Le Floc'h et al., 2005). 88% of the sources have a single counterpart in 2". We restrict the final sample to these objects with a single counterpart. The optical photometry is retrieved from the EIS data (Arnouts et al., 2001)

To build the sample at z=0.7 we selected galaxies in the redshift bin 0.6-0.8. We put a limit in luminosity to be complete in the redshift range and to avoid volume corrections. This limit is calculated for a limiting flux of 0.024 mJy at z=0.8, and translates to a total infrared luminosity $\log(L_{\rm IR}) = 10.34$ ($\rm L_\odot$) (see below for the calibration of the 24 μm flux in $L_{\rm IR}$). 280 sources are obtained that way (the faintest object has a 24 μm flux equal to 0.031 mJy). All these galaxies are detected with IRAC at 3.6 μm.

We must estimate the total infrared luminosity $L_{\rm IR}$ from 8 to 1000 μm to measure the "obscured" SFR. The extrapolation from the 24 μm emission alone to the total IR emission relies on local templates (e.g. Le Floc'h et al., 2005; Bell et al., 2005, 2007): tight relations have been found between the rest frame 12-15 μm and the total infrared emission of local galaxies (Chary & Elbaz, 2001; Takeuchi et al., 2005a). Recent studies based on SPITZER data suggest that there is not a strong evolution in the IR spectral energy distributions for intermediate redshift galaxies (Zheng et al., 2007b). At z=0.7, 24 μm corresponds to 14 μm and a calibration at 15 μm can be used. Takeuchi et al. (2005a) and Chary & Elbaz (2001) propose such calibrations. Here we use the relation of Takeuchi et al. (2005a) based on IRAS and ISO data and local templates from Dale et al. (2001) to be consistent with z=0 calculations. Using the Chary & Elbaz (2001) relation would lead to a slightly higher value of $L_{\rm IR}$ by 0.08 ± 0.01 in log units.

115 galaxies are detected at 2310 Å (NUV band from GALEX). At z=0.7 it corresponds approximately to the rest-frame FUV band of GALEX centered on 1530 Å (cf Buat et al., 2007a). In the same way, the 3.6 μm corresponds to a rest-frame K band. Therefore we can avoid K-corrections. For the galaxies detected at 24 μm, and in UV the SFR is estimated by combining the UV and IR emissions in a similar way to z=0 (Eq. 3). Since galaxies at higher z are more active in star formation than at z=0, we can expect a lower contribution of old stars to dust heating and hence a value of η lower than 0.3. To check this issue, we followed the method of Iglesias-Páramo et al. (2004) by comparing SFRs calculated with Eq. 3 to those deduced from the UV luminosity alone, corrected for dust attenuation using the recipe of Buat et al. (2005). The SFRs were found to be consistent if η=0; i.e., all the dust heating is attributed to young stars in these objects. Therefore we adopted η=0 to calculate the SFRs at z=0.7. For the galaxies not detected in the UV, the SFR was calculated with the IR luminosity only (again with η=0). The contribution of the UV emission at the detection limit of UV=26.2 mag is negligible in the estimation of the SFR (see section 4).

As for the z=0 samples, the stellar masses were estimated following Bell et al. (2003) who calibrate the M/L ratios as a function of several colors including those of the SDSS. The observed 3.6 μm band corresponds to the K band at z=0.7 and the observed R-I color from the EIS survey (Johnson-Cousin system) is similar to the u-g rest-frame color (from the SDSS). Therefore we used the u-g color-$\rm M/L_K$ relation of Bell et al. (2003) for the 305 galaxies with a R-I color. 18 galaxies have no R-I color so for them we used the mean $\rm M/L_K$ obtained for the sample i.e. $\rm M/L_K$=0.46 (solar units). The R-I color distribution is discussed in the next section.

2.2.2. UV-selected sample

GALEX (Morrissey et al., 2005) observed the CDFS for 76 ks in both the FUV (1530 Å) and the NUV (2310 Å) as part of its deep imaging survey. The reduction of the data is extensively described in Burgarella et al. (2007). Very briefly speaking, we used DAOPHOT to perform PSF-fitting and disentangle close neighbors. The completeness at a level of 80% was obtained at NUV=26.2 mag. The data are available from Burgarella et al. (2007). The cross-identification with the COMBO-17 sources is also described in Burgarella et al. (2007). About 70% of the GALEX sources are identified in COMBO-17 with a strong dependence on the NUV magnitude. Truncating at NUV=25.5 mag ensures us that more than 80% of the GALEX sources are identified. We adopt this limiting magnitude in the following and we restrict the final sample to objects with a single counterpart in COMBO-17 (90 % of the UV sources have more than one counterpart in COMBO-17). As for the IR selection to avoid volume corrections, we put a limit in luminosity, which ensures that we detect all the galaxies brighter than this limit in the redshift range 0.6-0.8. This limit is calculated for a magnitude NUV=25.5 at z=0.8. It corresponds to $\log(L_{\rm UV}) = 9.39$ ($\rm L_\odot$) and 247 galaxies are selected. 48% (119/247) of these sources are detected at

24 μm. For the undetected ones, we adopted an upper limit at 0.016 mJy, which corresponds to the detection limit at 3 σ (section 2.2.1). The IR luminosities $L_{\rm IR}$ were estimated from the 24 μm flux in the same way as for the IR-selected sample (section 2.2.1). The stellar masses were estimated in the same way as for the IR sample at z=0.7 and 230 galaxies have a R-I color. For the 17 remaining objects without a R-I color, we used the mean M/L_K obtained for the sample i.e. M/L_K=0.42 (solar units). The R-I color distribution will be discussed in the next section.

The star formation rate was estimated as for the IR selection when UV and 24 μm fluxes are available. We again took $\eta = 0$; this choice is also validated by the comparison between the SFRs calculated with Eq. 3 and $\eta = 0$ and those estimated from the UV luminosity corrected for dust attenuation (as for the IR selection, section 2.2.1). An upper limit on the SFR was calculated for the galaxies with only an upper limit at 24μm . This time we could not neglect the contribution of the IR emission which is dominant, even at the detection limit level (see next section).

3. Comparison of the UV and IR selections

Before discussing the star formation activity in both samples we analyze which selection (IR or UV) is best suited to our analysis. At z=0 Buat et al. (2007b) showed that the intrinsically brightest galaxies are lost in a UV selection. Conversely, intrinsically faint galaxies are hardly detected in IR. Because our present study is devoted to a comparison between low and higher z samples we do not discuss the intrinsically faint objects against which we are strongly biased (cf next section). At z=0, intrinsically bright galaxies are rare and the differences between both selections are small (Buat et al., 2007b); however, the galaxy population seen either in UV or in IR is known to brighten as z increases, we must also check the differences in the selections at z=0.7.

3.1. *The relative contribution of the IR and UV emissions to the bolometric luminosity of young stars*

At z=0 Buat et al. (2007b) compared the bolometric luminosities of the galaxies defined as $L_{\rm bol} = (1-\eta)L_{\rm IR} + L_{\rm UV}$. Briefly summarized, we showed that the UV luminosity alone is unable to reproduce the bolometric luminosity even for UV-selected galaxies and that the combination with the IR is mandatory. Once both luminosities are added to calculate $L_{\rm bol}$, a deficiency of very bright objects (in terms of $L_{\rm bol}$) is observed in the UV selection as compared to the IR one. Given the low number of such galaxies, these differences are slight as is shown in the next section, which is devoted to specific star formation rates.

In Fig. 1 we have plotted the IR to UV luminosity ratio versus $L_{\rm bol}$ for both samples at z=0.7. It can be seen that the IR luminosity is higher than the UV one for all the galaxies detected at both wavelengths since $L_{\rm IR}/L_{\rm UV} > 1$. The galaxies selected in UV and not detected at 24 μm exhibit the lowest bolometric luminosities with $L_{\rm bol} \leq 2.5\ 10^{10} L_\odot$ ($\log(L_{\rm bol}) \leq 10.4$). The galaxies selected in IR and not detected in UV span a very wide range of bolometric luminosity and hence of SFRs. The average trends found at z=0 are also reported in Fig. 1. The samples at z=0 and z=0.7 cover the same range of luminosity. The slight difference found in the distributions of the IR to UV luminosity ratio has been discussed in terms of dust attenuation by Buat et al. (2007a) (see also Burgarella et al. (2007)).

Some galaxies of the IR selection, detected in UV, do not appear in the UV-selected sample. The same is true for some galaxies of the UV selection that have an IR detection but are not included in the IR-selected sample: these "single" objects appear in Fig. 1 as simple crosses (IR selection) or "plus" symbols (UV selection) and represent 30% of both samples. Their presence is due to the method used to cross-correlate the data: for the IR (resp. UV) selection, the cross-correlation with the UV (resp. IR) sources is made using the complete list of the UV (resp. IR) detections before their identification with COMBO 17 objects and any other selection. The truncations to have complete volume-limited samples account for a half of the "single" objects. The other half of the IR (resp UV) "single" objects have a UV (resp IR) counterpart that has not been identified with a COMBO17 source. Such a rate of non-identification (15 %) is consistent with those quoted by Burgarella et al. (2007).

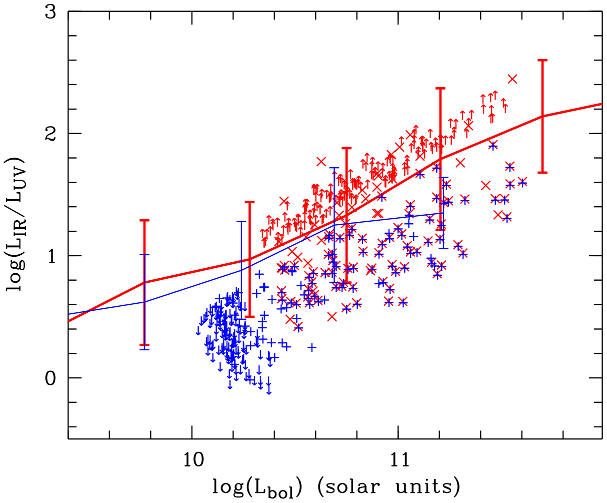

Fig. 1. IR to UV luminosity ratio as a function of the bolometric luminosity for both samples at z=0 and z=0.7. At z=0.7 individual data are plotted: UV selection with blue "plus" for galaxies also detected at 24μm and arrows down for galaxies not detected at 24μm; IR selection with red crosses for galaxies also detected at UV and arrows up for galaxies not detected at UV. At z=0 volume average trends (Buat et al., 2007b) are plotted with solid lines and error bars: the UV selection with a light solid line and the IR selection with a heavy solid line

3.2. *Color distributions*

It is well established that a population selected in optical or in NIR exhibits a bimodal distribution of colors. This result, first obtained at low z (e.g. Baldry et al., 2004), is also observed at higher z (e.g. Bell, 2004; Cooper et al., 2007; Bell et al., 2007; Elbaz et al., 2007). Blue galaxies are star-forming objects, whereas the redder ones are quiescent systems. Our galaxies were selected either in UV or in IR and so are likely to show active star formation. For the sake of comparison with other studies, we can check what sort of galaxies we are dealing with in terms of optical colors. Unfortunately for us, this check is very difficult to perform at z=0 since our sample was built from 2000 deg^2 not covered by homogeneous optical surveys like the SDSS. Nevertheless, we can rely on other studies of UV or

IR selected galaxies. Iglesias-Páramo et al. (2007) studied UV-selected galaxies from z=0.2 to z=0.7. The U-V distribution of their sample remains unimodal over the full redshift range they analyzed: according to the classical subdivision into blue and red galaxies, only blue star-forming galaxies are selected in UV. Goto (2005) studied the optical properties of a sample of galaxies selected from the IRAS catalog. The color distribution that he found is broad and extends from the blue peak to the red one defined from the SDSS studies.

At z=0.7 the situation is more favorable to our galaxy samples. We can work with the R-I color from the EIS catalog, which is similar to the u-g color in the rest-frame of the galaxies. The R-I color is converted in AB magnitudes according to the conversion formulae of Arnouts et al. (2001). The color distributions are displayed in Fig. 2. The distinction between red and blue populations is below and above $R-I \simeq 1$ (Elbaz et al., 2007).

The red population is under-represented for both selections but the two distributions clearly differ. As expected in UV we select preferentially blue galaxies that are active in star-formation. The selection looks similar to what is found by Bundy et al. (2006) for the DEEP2 survey restricted to galaxies with a SFR larger than 0.2 $M_\odot yr^{-1}$ measured with the [OII] equivalent width. The distribution of the IR-selected galaxies is broader and shows a tail towards redder objects, but we do not see any clear bimodality as reported for example for optically selected galaxies (see references above). This agrees with the findings of Bell et al. (2005) at a similar redshift that the galaxies detected at 24 μm are spread over a wide range of optical colors. If we compare, for example, to the distribution of Elbaz et al. (2007) it seems that our distribution is broader with a substantial fraction of our sample between the two peaks defined in U-B rest-frame (similar to observed R-I at z=0.7). Therefore a selection at 24 μm does not exhibit bimodality, and it also seems to be the case at z=0 for galaxies selected from IRAS: IR-selected galaxies seem to populate the “green valley” located between the blue and red peaks. A substantial fraction of these galaxies with intermediate colors exhibit a strong dust attenuation with the IR to UV flux ratio greater than 10 and they are often not detected in UV (cf Fig. 1). It may be noted that the fraction of non detections does not vary a lot with the bolometric luminosity of the galaxies. The IR selection does not include the large number of very blue galaxies detected in the UV with low bolometric luminosity (cf Fig. 1). Last of all, when only galaxies selected at both wavelengths are concerned (dashed histograms) the properties of both samples are found to be similar, it is also clearly seen in Fig. 1.

4. Specific star formation rates

4.1. Variation in the SSFR within each sample

In this section, we analyze the variations in the specific star formation rates (SSFR, defined as the total SFR divided by the stellar mass) as a function of the stellar mass within our samples of star-forming galaxies. In Fig. 3 the SSFRs versus stellar masses are plotted for both samples at both redshifts. Average trends are plotted at z=0. They come from Buat et al. (2007b) where volume averages were performed. The values were converted using the SFR and stellar mass calibrations adopted in this paper (section 2.1). At z=0.7, the values for each galaxy are plotted.

Before any interpretation, we must estimate the detection limits in SSFR to determine where the results are reliable, on the basis of the limiting fluxes adopted in UV and IR. Stellar masses were estimated from the 3.6 μm flux, available for each galaxy, and are thus unaffected by detection limits. Practically speaking, for the IR selection we adopt the limit of $\log(L_{\rm IR}) = 10.34$ ($L_\odot$) used to build the sample (cf section 2.2.1) and translated it into SFR at z=0.7 with Eq. 1. We obtain $SFR_{\rm lim} = 2.34\ M_\odot yr^{-1}$. Given the high values of the IR to UV ratio for the IR selection (cf Fig. 1), we have neglected the contribution of the UV emission to estimating $SFR_{\rm lim}$. For the UV selection, the adopted limit $\log(L_{\rm UV}) = 9.39(L_\odot)$ translates into an “unobscured” SFR at z=0.7 of 0.50 $M_\odot yr^{-1}$ according to Eq. 2. However we must also account for the contribution of the IR emission to the SFR which is not negligible at all (cf Fig. 1). We used the detection limit of 0.016 mJy at 24 μm (cf. section 2.2.1) translated into an “obscured” SFR at z=0.7 of 1.15 $M_\odot yr^{-1}$. The limit thus obtained for the total SFR is $SFR_{\rm lim} = 1.65 M_\odot yr^{-1}$. The resulting detection limits obtained for z=0.7 for the SSFRs (and only constrained by those on the SFR) are reported in Fig. 3.

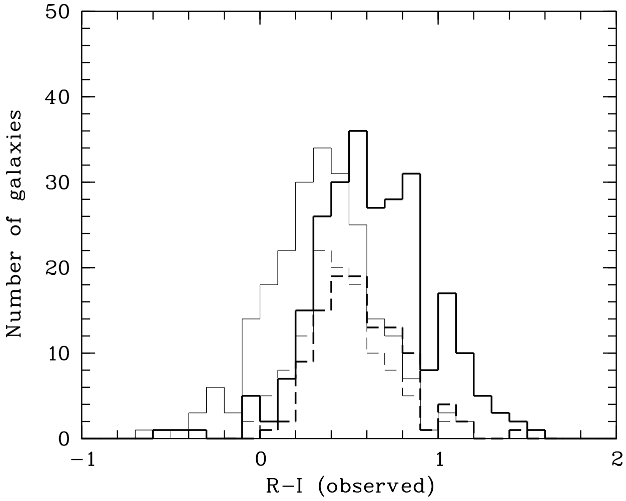

Fig. 2. Observed R-I color (AB scale). Heavy solid line: whole IR selection, heavy dashed line: IR selected galaxies also detected in UV. Light solid line; whole UV selection, light dashed line: UV selected galaxies also detected at 24 μm

The z=0 samples are purely flux-limited so we cannot estimate the detection limits in the same way as for the z=0.7 sample. Buat et al. (2007b) built bolometric luminosity functions with these samples ($L_{\rm bol} = L_{\rm UV} + (1-\eta)\ L_{\rm IR}$) down to 6.3 $10^8\ L_\odot$ and 1.8 $10^9\ L_\odot$ for the UV and IR selections respectively. These luminosities were used to estimate the limits reached in SFR and they can be translated in SFR using Eq. 1. We obtain $SFR > 0.07 M_\odot yr^{-1}$ for the UV selection and $SFR > 0.19 M_\odot yr^{-1}$ for the IR selection. Such low SFRs put detection limits well below the values reported in Fig. 3 for the mean trends at z=0.

The influence of the choice of η (Eq. 3) can be easily checked: the measure of the SFR is mostly dominated by the IR emission with only a small contribution from the UV one, especially for massive galaxies which will be the main topic below. Therefore adopting $\eta = 0.3$ instead of $\eta = 0$ at z=0.7 will reduce the SFR and hence the SSFR by a factor 0.7, i.e. a translation of -0.15 dex on the vertical axis of Fig. 3.

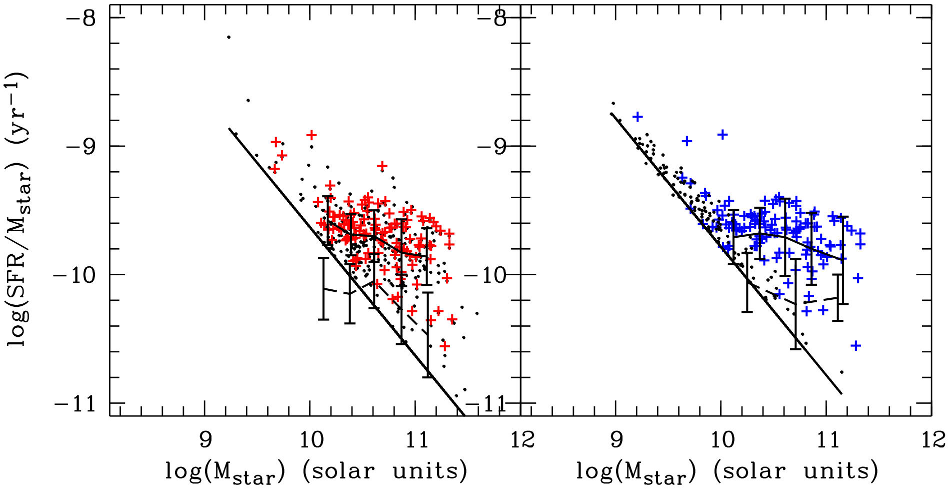

Fig. 3. SSFR versus stellar masses. Left panel: IR selection, the z=0.7 galaxies detected at 24 μm and in UV are plotted with red crosses, the galaxies only detected at 24 μm with dots. The solid line with error bars (1 σ) is the result of the volume average at z=0.7, the dashed line the volume average at z=0. The diagonal line represents the detection limit at z=0.7. Right panel: Same plot for the UV selection. At z=0.7 galaxies detected at 24 μm and in UV are plotted with blue crosses, the galaxies only detected at UV with black crosses, the lines are defined in the same way as for the IR selection. Adopting η=0 instead of η=0 at z=0.7 would shift all the data at z=0.7 by -0.15 dex along the vertical axis

It is obvious from Fig. 3 that the locus of the galaxies with masses lower than 10^{10} M$_\odot$ is completely governed by detection limits at z=0.7. The observed trends are only reliable for $M > 10^{10}$ M$_\odot$. In the following, we limit our analysis to this mass range. The trends found for both selections seem to be similar, they will be compared in the next sections.

Our samples were built to be complete in terms of the star formation rate (as discussed above in this section) but are not expected to be complete in mass. Indeed a mass-selected sample also contains quiescent galaxies that are not present in our sample. At z=0 we built the stellar mass function using the V/V$_{max}$ formalism for the IR and the UV-selected samples. They are compared to the stellar mass functions derived by Bell et al. (2003) from SDSS+2MASS data. We have applied the correction preconised by Bell et al. (2003) for a Kroupa IMF. As expected, the stellar mass distribution of the UV-selected sample is similar to what is found by Bell et al. (2003) for late-type galaxies (selected according to their colors), whereas the IR selection leads to a larger number of massive galaxies but still below the total stellar mass distribution. At z=0.7 we can directly compare the counts obtained for a selection at 3.6 microns (IRAC), 24 microns (MIPS), and in NUV (GALEX) for the redshift bin 0.6-0.8. Fig. 5 summarizes the comparison where the counts are reported against the stellar mass. The selection at 3.6 microns consists of sources brighter than 3 μJy, which corresponds to 10^{10} M$_\odot$ at z=0.7; this limit is very conservative given the depth of the IRAC observations (Elbaz et al., 2007; Sanders et al., 2007). Both MIPS and GALEX selections lead to lower counts than the IRAC one. The effect is more extreme for the UV selection. This was expected from Fig.1 where it is obvious that the UV selection misses bright (and therefore massive) galaxies with a substantial dust attenuation. Conversely the contribution of the UV sources becomes significant for masses around 10^{10} M$_\odot$. We have also included in Fig. 5 galaxies selected in either the UV or the IR in order to analyze their total mass distribution. The difference between the number of galaxies in our GALEX+MIPS selections, and the IRAC one is likely to be due to the presence of quiescent systems detected neither at 24 μm nor in NUV. It is qualitatively consistent with the relative contribution of spirals and irregulars to the total stellar mass function as measured by Bundy et al. (2005) in the same redshift range. A full analyzis of the luminosity functions in our selected samples is in preparation (Takeuchi et al.).

Before comparing to models we also calculate average trends at z=0.7 (Fig. 3). There is no need for volume corrections (cf section 2.2) and simple mean values can be calculated. We have used the Kaplan-Meier estimator for the IR selection and the error bars plotted in Fig. 3 correspond to the 1σ dispersion. For the UV selection, the presence of upper limits located on one side of the distribution hampers the use of the Kaplan-Meier estimator. Therefore we have calculated the median instead of the mean for the UV selection at z=0.7. Very similar trends are found in both selections (see also Fig. 7 where average trends for both selections are overplotted). Even if the UV selection misses highly reddened galaxies (cf Fig. 1), the star formation activity of the galaxies selected in UV is found to be similar to those selected in IR: the SSFRs do not depend critically on the adopted selection (as long as they are estimated by combining UV and IR emis-

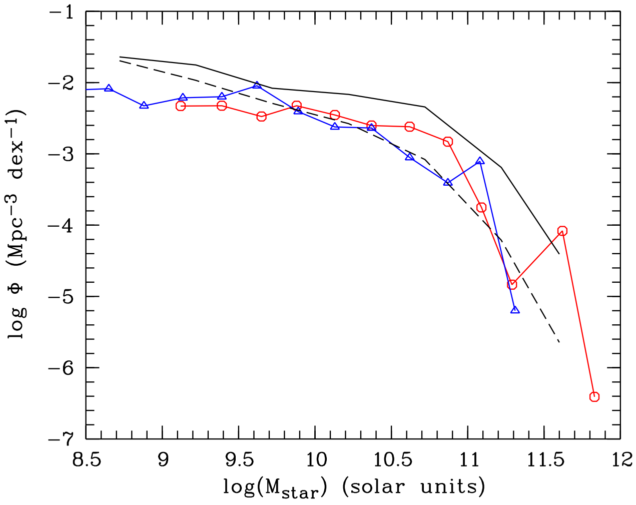

Fig. 4. Stellar mass functions for the z=0 samples selected in IR (circles) and in UV (triangles). The solid line without symbols is the total stellar mass function derived by Bell et al. (2003) and the dashed one denotes the stellar mass function for late type galaxies by the same authors

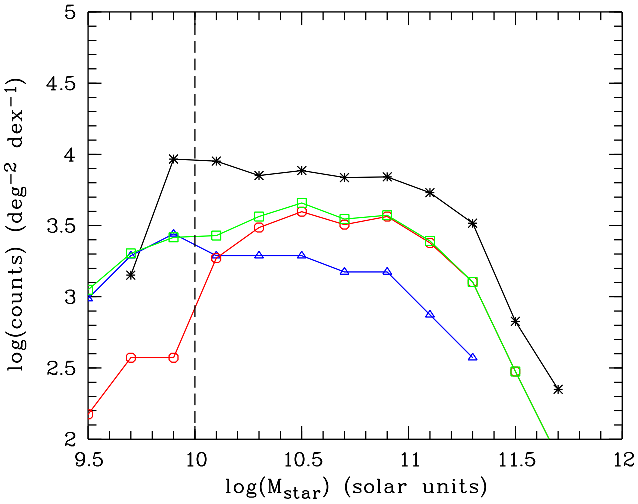

Fig. 5. Galaxy counts as a function of the stellar mass for a selection at 3.6 μm (stars), 24 μm (circles), in NUV (triangles) and for the galaxies selected either at 24 μm or in NUV (squares)

sions), a result already found at z=0 once volume corrections are applied to the local samples (Buat et al., 2007b, and Fig. 7).

4.2. Comparison with previous studies at intermediate redshift

Numerous works address the question of the variation in the specific star formation rate at various z. Whereas these studies conclude to a general decrease of the SSFR with galaxy mass even at high z (the so-called downsizing effect), the trends exhibit large departures from one work to another. Our aim in this section is not to perform an exhaustive comparison with all the available results: we will instead discuss a few studies performed in the same redshift range as the present work, and using methods to estimate SFR and stellar masses similar to ours.

Zheng et al. (2007a) analyzed the dependence of star formation on galaxy mass within the COMBO 17 survey adding SPITZER data to measure accurate SFRs. The SSFRs they reported are consistent with ours within error bars but with a steeper decrease in the SSFR when stellar mass increases compared to what we find. Their sample contains blue and red galaxies, Bell et al. (2007) considered them separately and found a flatter distribution of SSFR for the blue ones than for the red ones. In a similar way Elbaz et al. (2007) analyzed the GOODS survey and found a flat distribution of SSFRs at z=0.8-1.2 and between 10^{10} and 10^{11}M$_\odot$. The decrease in the SSFR they found around 10^{11}M$_\odot$ is clearly due to the red galaxies, whereas blue galaxies exhibit a roughly constant SSFR (their figure 17).

Noeske et al. (2007) also found a flat distribution that is fully consistent with ours within the AEGIS survey (both in absolute values and trends) for galaxies with stellar masses between 10^{10} and 10^{11}M$_\odot$ and more massive galaxies have a lower SSFR. Studies based on GALEX data and combining UV and IR emissions have also led to an almost flat distribution of SSFRs. Iglesias-Páramo et al. (2007) performed a UV selection combined with SWIRE data from z=0.2 to z=0.7 and found a flattening of the SSFR versus M$_{star}$ variation from z=0.2 to z=0.7. Martin et al. (2007) also found a flat distribution in the CDFS at intermediate z with deep GALEX and MIPS data. Zamojski et al. (2007) perform a very complete analysis of the COSMOS field (although only based on UV-optical rest-frame data) at z=0.7. Their UV-detected sample also exhibits a rather flat distribution of SSFR, much flatter than obtained for their entire sample (including objects not seen in UV).

Although a large dispersion is found in the already published results, we find good agreement with those focusing on star-forming galaxies alone. The steeper decrease in the SSFR with increasing mass found in some studies at intermediate redshift is likely to be due to the presence of quiescent systems, which are absent in our present selection (e.g. Bell et al., 2007; Elbaz et al., 2007). Similar differences are found at z=0 when only star-forming galaxies are selected or quiescent are also added (Brinchmann et al., 2004; Buat et al., 2007b; Elbaz et al., 2007). Most of the decrease found at z=0.7 also occurs for masses higher than 10^{11}M$_\odot$ (e.g. Zheng et al., 2007a; Noeske et al., 2007; Elbaz et al., 2007) which are not well represented in our sample.

5. The models

Recent studies have found evidence of the minor role of strong mergers in the evolution of massive galaxies from z=0 to ∼ 1 (Bell et al., 2005; Melbourne et al., 2005; Zheng et al., 2007b). Therefore it is tempting to try to fit the data with models that assume a smooth average evolution, which is weakly challenged by small interactions and minor mergers.

Table 2. Models with λ = 0.05, z_f = 6, stellar masses are calculated at z=0 (column 2) and z=0.7 (column 3) with the analytical fit

velocity (km s^{-1})	$\log(M_{\rm star})_{z=0}(M_\odot)$	$\log(M_{\rm star})_{z=0.7}(M_\odot)$	a	b	c
80	8.89	8.19	6.62	0.41	0.36
150	9.92	9.51	8.74	0.98	-0.20
220	10.52	10.25	10.01	1.25	-0.55
290	10.94	10.75	10.81	1.35	-0.74
360	11.25	11.10	11.35	1.37	-0.85

Recently Noeske et al. (2007) proposed a simple model of gas exhaustion to interpret the variation in the SFR as a function of the stellar mass out to z=1.1. In their model galaxies experiment exponential star formation histories with e-folding rates and redshift formation varying with the galaxy mass, less massive galaxies being younger and having higher e-folding rates.

Here, instead of building ad hoc models (the parameters in Noeske et al., 2007, are fine-tuned for their data) for our study, we follow a "backward" approach (e.g. Silk & Bouwens, 1999) by starting from studies of the Milky way and the nearby universe to extrapolate the behavior of galaxies at higher z, without any further adjustment of the models that are constrained in the local universe (see details below).

5.1. Description of the models

To interpret our results with physically motivated models, we use a grid of models for the evolution of spiral galaxies that is similar to the one presented in Boissier & Prantzos (2000). These models were calibrated to reproduce many properties of the Milky Way (Boissier & Prantzos, 1999), and were compared to nearby spirals in subsequent works. They should be adequate to broadly represent the family of spirals from very massive ones to irregular low-mass exponential disks. The models use scaling relationships to simulate disks of various rotational velocity and spin parameter (λ, measuring the specific angular momentum, see e.g. Mo, Mao & White, 1998, for a definition). The velocity is closely related to the total mass of the galaxy and, as a result, its final stellar mass. Each stellar mass (at any redshift) corresponds to one and only one model for a given specific angular momentum λ. The specific angular momentum has a log normal distribution (e.g. Mo, Mao & White, 1998). Spirals have spin parameters between 0.02 and 0.08, with a typical value of 0.05 (the Milky Way Galaxy corresponding to $\lambda \sim 0.03$ in Boissier & Prantzos, 2000). Since we are interested in general trends with mass, we only use models with this average λ =0.05 in the following. The quantities we present in this paper present, in any case, a much stronger dependence on the velocity than on the spin parameter.

The models assume that galaxies are formed by progressive infall of primordial gas, starting at high redshift ($z_f = 6$). Models of the Milky Way shown early-on that infall of "fresh" gas provides a good explanation especially for the distribution of metallicity of G-Dwarfs in the Solar neighborhood and the idea has been widely used (e.g. Larson, 1972; Pagel, 1997; Chiappini et al., 1997; Boissier & Prantzos, 1999). Such models do not state that this gas has been forever in a reservoir around the galaxy. In a more modern context, it could very well be that this infall corresponds to small satellites (with large gas fraction) being accreted by the galaxy during minor mergers. Inside the disk, stars form from the gas following a Schmidt-like law, including a dynamical factor. In a recent work (Boissier et al., 2003), the star formation law was empirically determined to be

$$\Sigma_{\rm SFR} = 2.63\,10^{-3}\Sigma_{\rm GAS}^{1.48} V(R)/R \tag{4}$$

relating the surface density of star formation rate $\Sigma_{\rm SFR}$ ($M_\odot pc^{-2} Gyr^{-1}$) to the gas surface densities $\Sigma_{\rm GAS}$ ($M_\odot pc^{-2}$). Here $V(R)$ is the rotation velocity (km s^{-1}) at radius R (kpc). This formulation is very close to the one originally used, and subsequent models (including in this paper) have used it. The results are very close to those in Boissier & Prantzos (2000), and show the same global trends.

The star formation history in these models strongly depends on the built-in assumption that infall proceeds at a higher pace early in the history of massive galaxies with respect to the Milky Way, and later in lower mass galaxies. This assumption corresponds to the so-called "downsizing" effect, and was made to adequately reproduce observed trends in nearby spirals.

By construction, these models should match the z=0 universe at the current epoch. The use of such models in a backward approach is indeed justified only because a very large number of properties of nearby galaxies (i.e. the redshift zero universe) are correctly reproduced by them. It is notably the case (and we refer to the references for further details) of scaling relationships such as surface brightness and scalelength versus magnitude, the Tully-Fisher relationship (and its dependence on wavelength), color-magnitude diagrams (B-K vs K), luminosity-metallicity relationship, spectra (Boissier & Prantzos, 2000), colors and abundance gradients in spirals (Prantzos & Boissier, 2000), star formation rates and gas fractions (Boissier et al., 2001).

In a "backward" approach, their prediction about the past was only compared to a few properties of small samples of spirals at higher redshift (Boissier & Prantzos, 2001), and no serious discrepancies were found with the data available at the time. Note that the observed B-band luminosity function at redshift zero was reproduced by the models in this paper. This result was obtained by construction since the authors assumed a circular velocity distribution V_C derived from observations, and the models reproduced the M_B vs V_C relationship.

We propose here to use these models to interpret data concerning the SSFR (such data did not exist a few years ago).

5.2. Star formation histories

The star formation histories (presented in Fig. 6, left panel) of the models result from the non linear combination of a star formation law, an infall history and its mass dependence. To provide an easy way to compare our star formation histories to others, or to various data sets, we propose an analytical form for the star formation history of our models. After testing several possibilities, we obtained a correct fit using three parameters:

$$SFR(t) = At^b \exp(-(t/\tau)^{0.5}) \text{ or} \tag{5}$$

$$\log(SFR(t)) = a + b\ \log(t) + c\ t^{0.5} \tag{6}$$

$$\text{with } a = \log A \quad c = -0.43\tau^{-0.5}. \tag{7}$$

We can assign a tentative physical significance to each of the parameters : A is a scaling factor, b is measuring the rate at

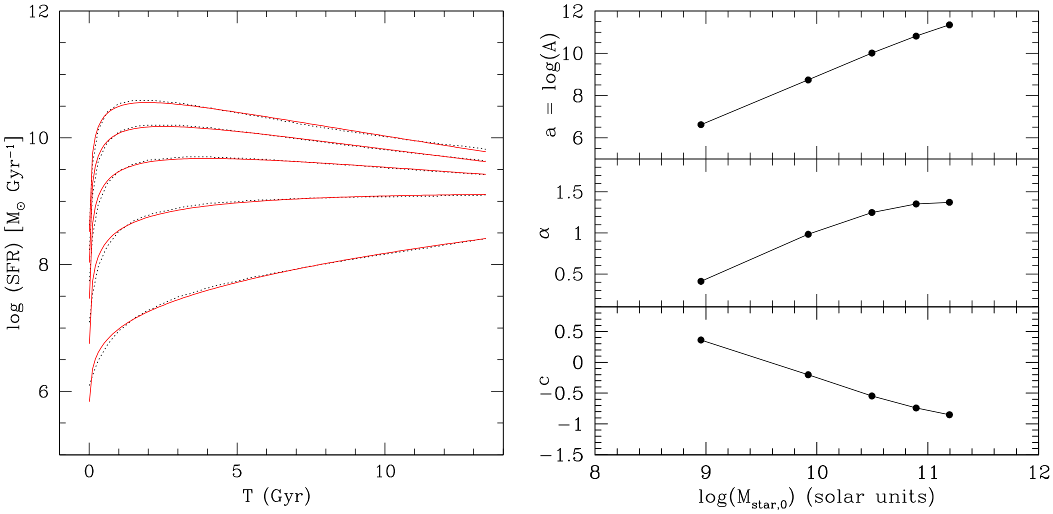

Fig. 6. Left: Star formation histories of the adopted models for five final stellar masses (equivalently: five rotational velocities), from the lowest mass (bottom) to the highest one (top). The dotted line is the result of computing of the chemical evolution models and the solid line is the analytical fit of (Eq. 6). On the x-axis, T=0 Gyr corresponds to the formation of the galaxies ($z_f = 6$), z=0.7 corresponds to T = 6.2 Gyr and z=0 to T = 12.5 Gyr. Right: Variation in the three parameters (a,b,c) of the analytical star formation history (Eq. 6) as a function of the present (z=0) stellar mass (values are given in Table 2 for the five models shown on the left, also shown as dots in this panel).

which the star formation increases early-on, and τ is a time-scale for the decay of star formation at later time (this is not always the case: for low-mass galaxies the star formation rate is still rising at late epochs). The values of these parameters for the $\lambda = 0.05$ models are given in Table 2 for a few values of the circular velocity and their dependence on the final (z=0) stellar mass is shown in Fig. 6 (right panel). The quality of the fit can be judged from the left panel. With such a formula, it is straightforward to compute analytically the evolution of stellar masses assuming the instantaneous recycling approximation (e.g. Pagel, 1997) and a returned fraction of R=0.3 for the Kroupa et al. (1993) IMF (Boissier & Prantzos, 1999). We checked that this simple approach gives a very good approximation to the results of the numerical computations implementing infall, star formation law, and finite lifetimes of stars.

Before comparing the models and the data, we should note that some ingredients of the chemical evolution models are rather uncertain. Especially, the star formation law efficiency is very dispersed among disk galaxies, making the star formation rate uncertain by about a factor 2. In addition, we used the Kroupa et al. (1993) IMF, for consistency with earlier works. We checked that if we used the more recent Kroupa (2001) IMF for the models, the star formation rate and stellar mass during the overall history of the galaxy would change by only 10 to 20 %. Modifying the IMF from Kroupa et al. (1993) to Kroupa (2001) mainly affects the population of massive stars and, as a consequence, the calibration of the current star formation rate and the predicted UV fluxes is why we use the more recent IMF (Kroupa, 2001) to derive SFR from the UV fluxes (Eq. 2). Model predictions other than UV fluxes depend much more weakly on this choice.

Hammer et al. (2007) suggest that the Milky Way, having escaped significant merging over the last ~ 10 Gyr, is in fact unrepresentative of spirals in contrary to M31. Our models, even if they were calibrated in the Milky Way, successfully reproduced many properties of nearby spirals, including abundance and colour gradients (Boissier & Prantzos, 2000; Prantzos & Boissier, 2000). The star formation law (the "Schmidt"-like law mentioned above) was determined from 16 galaxies with Hα profiles (Boissier et al., 2003), and is consistent with the SFR indicators in the Milky Way. The SFR profiles have been determined in 43 nearby spirals from UV data (Boissier et al., 2006) and compared to gas profiles. The SFR-gas connection they find agrees with the one derived from Hα profiles, even if the relationship extends to lower gas surface densities in the UV (the untypical galaxy with this respect was actually M31, which does not follow the Schmidt law in its inner part). We recognize that the models calibrated in a relatively calm Milky Way probably not include all the details of disk galaxy evolution. However, they do agree with many properties in nearby spirals as discussed above and we believe they reproduce the major traits of disk evolution even if real galaxies are likely to sometimes suffer interactions not taken into account in this approach (as long as they are not dramatic events destroying the disks such as major mergers.

6. Results and discussion

6.1. Comparison between models and data at z=0 and z=0.7

In Fig. 7, the results of the model are compared to the mean observational trends obtained in section 4. The agreement can be considered as good for both selections at $M > 10^{10}$ M$_\odot$ given the large intrinsic dispersion of the data and the fact that no fitting has been performed. At z=0.7 the agreement is remarkably good given the uncertainties inherent to both the models and the data (see the discussion below). At z=0 the SSFRs predicted by the model lie slightly above most of the mean observed values and exhibit a steeper decrease as the stellar mass increases, as compared to the UV selection, although the intrinsic dispersion of the observed quantities is very large. As discussed in section 5.2, models themselves contain some uncertainties. Modifying the star formation law efficiency within the uncertainties could modify the star formation rate by a factor ~2, and various IMF may modify the results of the models by up to ~ 20 % as seen above. The models errors are likely to be systematic if the IMF and the star formation are universal, i.e. directly linked to the physics of star formation on a local scale rather than depending on the global properties of galaxies. In that case, the trends obtained by the models are robust even if the absolute values could change.

Models predict directly the stellar masses, their estimates do not depend on any assumed mass-to-light ratio. The uncertainty on the mass-to-light ratios only affects the masses derived from the observations. It can reach a factor 2 (Kannappan & Gawiser, 2007), similar to the dispersion found for the observed SSFRs for a given range of stellar mass. Therefore both models and observables are likely to be affected by systematic errors large enough to explain the slight shift found at z=0 between the models and the data in Fig. 7. Another issue may be that the SSFR trend with the stellar mass is flatter for the UV-selected sample than the models predictions. Indeed the UV selection leads to a selection of late-type systems (cf section 4.1 and Fig. 4); and since the contribution of early type galaxies increases with the stellar mass (Fig. 4), we expect a flatter distribution of the SSFR for the late type systems alone as compared to the total galaxy population. The models are set up to reproduce the mean evolution of galactic disks. For massive galaxies, they correspond to relatively early disk types (as early as Sa) in which the specific star formation rate is low: i.e., the star formation activity is low.

The UV selection can pick up massive galaxies with active star formation due to burst or refueling through interactions (leading to later type galaxies for the same mass) not introduced in the models that then correspond better to the galaxies from the IR selection (picking up massive galaxies with more quiescent star formation).

At higher z, because of the higher star formation activity in all the galactic disks, this effect is expected to be smaller and the discrepancy between the models and the data disappears.

Noeske et al. (2007) have performed a similar analysis to ours. They selected galaxies between z=0 to z=1 from the AEGIS survey. They derived SFR by combining IR, optical, and UV data. Their SSFR distributions are very consistent with ours. As a result, the gas exhaustion model they propose would also fit our data reasonably well. In their model, star formation rates follow an exponential decay after a formation redshift z_f. Less massive galaxies have a longer e-folding rate and a lower redshift of formation. Nevertheless, it implies a wide range of redshift formation, from z_f=1 for 10^{10}M$_\odot$ up to z_f=3 or 10^{11}M$_\odot$. In our model, on the contrary, all the galaxies have the same formation redshift $z_f = 6$, which is the epoch when galactic building blocks are assumed to start to exist. It is roughly the redshift when the first galaxies are confirmed to exist (e.g. Schaerer, 2007). In this approach, it is the time variation of the SFR that depends on the galaxy mass, in such a way that the bulk of star formation occurs at different ages according to the galaxy mass. Actually, the star formation histories obtained in our models are qualitatively similar to the schematics proposed by Sandage (1986), which inspired more recent works. Among them, Gavazzi et al. (2002) used a star formation history law “a la Sandage”, which is mimicking the Sandage (1986) trends. Quantitatively, our star formation history is slightly different: for massive galaxies especially, the SFR does not decrease as quickly at late epochs.

Because of this, the mean evolution of the SSFR from z=0 to z=0.7 in star-forming galaxies of $10^{10} - 10^{11}$M$_\odot$ is consistent with the one predicted by a simple but physically motivated model of secular evolution, in which the galaxies are progressively built by accretion of low-metallicity gas and in which star forms according to a “universal” law of star formation. It does not mean that individual galaxies cannot experience any burst events or interactions, but our aim is only to reproduce mean trends. At z=0, active galaxies were found in the IR selection (Buat et al., 2007b), but these objects were also diluted among the more numerous fainter objects when volume averages were performed. In the same way the most active galaxies of our samples at z=0.7 have SFRs reaching 40 M$_\odot$ yr^{-1}, a factor ~ 2 larger than highest SFR from our models (Fig. 6). Indeed luminous infrared galaxies (LIRGs which account for 30 % of our IR selection) are known to experience bursts (e.g. Marcillac et al., 2006). Nevertheless when averages are calculated their influence is diluted. Indeed, our results do not imply a secular evolution for the whole galaxy population but are instead consistent with a smooth mean evolution in agreement with the idea that galaxies are built by infall (which can be in the form of minor mergers, as suggested above). In this context, major mergers or other extreme events are not expected to participate much in the construction of the average galaxy.

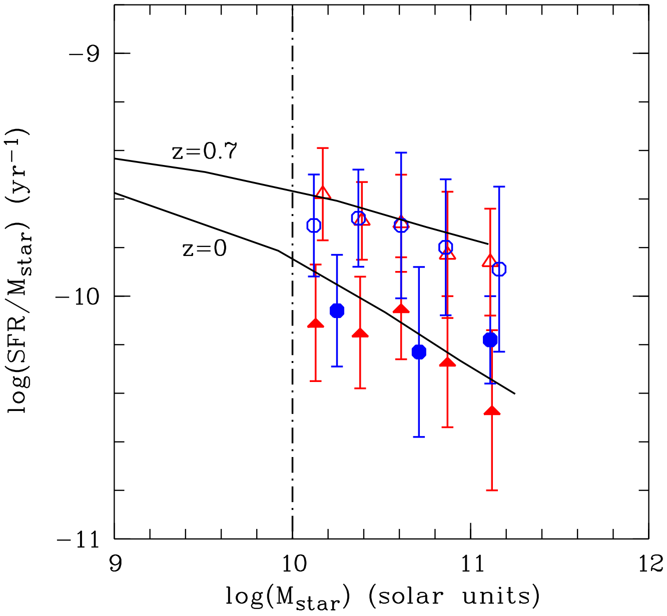

Fig. 7. Specific SFRs versus the stellar mass: comparison between data and model. UV selection: blue circles and error. IR selection:red triangles and error bars. The filled symbols are for z=0, the empty ones for z=0.7. The solid lines represent the model summarized in Table 1 (see text)

Interestingly, the model with a circular velocity of 220 km/s, corresponding to the one of the Milky Way, has a stellar mass of $\log(M_{\rm star}) = 10.52$ (M$_\odot$) at z=0 and $\log(M_{\rm star}) = 10.25$ (M$_\odot$) at z=0.7. In other words, our samples probe Milky Way analogues in terms of stellar mass.

6.2. Comparison with semi-analytical models

The models presented above have the advantage of reproducing many properties of galaxies at redshift zero. They assume smooth evolutions on average, which might not be realistic in the paradigm of hierarchical galaxy formation. Semi-analytical models (SAMs) usually follow a similar approach to our models (e.g. assuming empirical recipes for star formation laws and scaling relationships) but obtain the mass accretion and merging histories of the galaxies by following the hierarchical growth of dark haloes (and the baryonic galaxies within them).

We also compared our data to the results of two sets of SAMs. Kitzbichler & White (2007) have produced lightcones simulations that can be very conveniently compared to observations. They applied the SAM of Croton et al. (2006) to the Millennium Run simulation (Springel et al, 2005). Nagashima et al. (2005) have constructed a numerical catalog also based on SAMs and combined with high resolution N-body simulations. We have applied selections to these simulated catalogs as close as possible to those obtained for our observational data (section 4.1): an SFR higher than 2 $M_\odot$ yr^{-1} for galaxies at a redshift between z=0.6 and 0.8 and an SFR higher than 0.1 $M_\odot$ yr^{-1} for nearby galaxies ($z < 0.1$). We computed average trends with the simulated data in the same way as in section 4 for our observational datasets. The results are displayed in Fig. 8, where the simulated quantities are compared to our mean observational trends obtained for the IR and UV selected samples. It can be seen that the simulated data also reproduce the values of the mean SSFR observed at z=0.7, although the simulations lead to a somewhat steeper decrease in the mean SSFR towards high stellar masses than observed. A rather large discrepancy is observed at z=0 for the millennium simulations: the simulated galaxies have lower SSFRs than the values measured in our samples. If we ignore this discrepancy the agreement is satisfactory. We can conclude that SAMs present a similar mean behavior to the one found for our simpler evolution model aimed at reproducing present day spirals without strong merger events. This result reconciles backward and forward approaches for the evolution of galaxies at least until z=0.7 and validates our simple approach for star-forming galaxies.

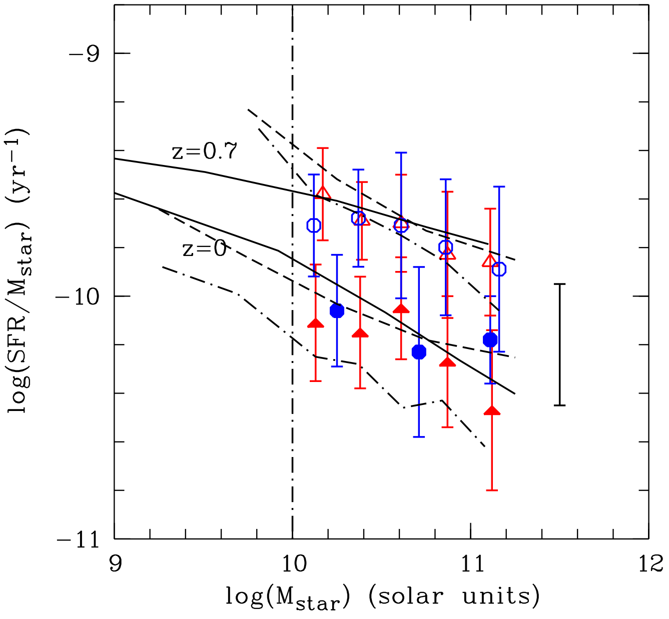

Fig. 8. Predictions of the Millennium model at z=0.7 and z=0 (dot-dashed lines) and of the numerical catalog of Nagashima et al. (2005) (dashed lines). All the other lines and symbols are the same as in Fig 7. The mean error bar (1σ) is indicated on the right side of the panel

The SAMs should be able to reproduce galaxies with very high SSFR induced by major mergers, whereas our model only aims at reproducing mean trends. Nevertheless, it may be meaningful to mention that the timestep used in the simulation (about 300 Myr for the Millennium simulation (Kitzbichler & White, 2007)) might be too large to catch short time bursting systems and the SFRs averaged over such a time step cannot be very high. This aspect of the simulation works should be improved in order to make a more extensive comparison of star-formation related quantities, like SSFR. A more exhaustive discussion of the results of semi-analytical simulations is beyond the scope of this paper and will be shown elsewhere.

6.3. Predictions and comparison with data for higher z

Since our models are able to reproduce the evolution of massive star-forming galaxies from z=0 to z=0.7, we can take a step further and make some predictions at higher z. These predictions can be considered as a reference for quantifying the expected properties of distant galaxies in the absence of major merging, implying a strong starburst and a very high efficiency of star formation. In Fig. 9 are reported the evolution up to z=4 of the SSFR and of the gaseous phase metallicity of the chemical evolution models.

6.3.1. Redshift evolution of the specific star formation rate

A main prediction issuing from such a secular evolution is the reduction in the range of values of the SSFR when the redshift increases (Fig. 9, panel a). This is a natural result because for a hypothetical first generation of stars formed during a brief time δt, we should have $SFR \times \delta t \sim M_{\rm star}$. Equivalently the model predicts a flattening in the variation of the SSFR as a function of the stellar mass as z increases (Fig. 9, panel b). Such a flattening is indeed observed in our data up to z=1 and in other studies (Iglesias-Páramo et al., 2006; Martin et al., 2007)

At high z, very few observational studies exist. Moreover they are often difficult to compare because selection effects are likely to become extremely strong. For example a K selection at z=4 corresponds to a B rest-frame one. Feulner et al. (2005) analyzed the FORS Deep Field and GOODS-S field to derive the variation in the SSFR up to z=4 for different ranges of stellar mass from an I and a K selection. Their average values for intermediate mass systems ($10^{9.5} - 10^{10.5} M_\odot$) are in reasonable agreement with our models from z=1 to z=3. In all the redshift range they explore, Feulner et al. (2005) find a strong decrease in the SSFR as the mass increases, which might seem at odds with the predictions of our model (Fig. 9, panels a & b). However, Feulner et al. (2005) did not select only star-forming galaxies, and the contribution of quiescent objects can steepen the variation in the SSFR with the mass since they are essentially very massive objects. Indeed very recently Daddi et al. (2007) studied star formation in massive galaxies forming stars actively up to z~2 and found a roughly constant SSFR at z=2 for galaxies detected at 24 μm and with a mass comprised between $\sim 5\,10^9$ and $\sim 10^{11}$ $M_\odot$, in agreement with the predictions of our model. Daddi et al. (2007) find an increase in the SFR at a given mass from z=0 to z=1 and z=2 by a factor ~4 between z=1 and 2 and a factor ~30 between z=0 and 2, these values are higher than those we predict (a factor ~2.5 between z=1 and 2 and a factor ~10 between z=0 and 2).

Lamareille et al. (2007) present the variation in the SSFR up to z=2.5 for the VIMOS VLT Deep Survey in different bins of stellar mass. The absolute values, as well as the variation they found for the galaxies with $10 < \log(M_{\rm star}) < 11$, are very consistent with our models. From their Fig 2 there is also a hint of some flattening of the SSFR-$M_{\rm star}$ variation when z increases but still of a decrease in the SSFR as the mass increases. As in the case of the study of Feulner et al. (2005), the VVDS is an I band selected survey that might not only select star-forming galaxies but also more quiescent objects: a steep decrease in the SSFR with increasing stellar mass is expected with a bimodal galaxy population.

SAMs have been used in the literature to compare to observational sets in the same way we proceeded at z=0.7. Daddi et al. (2007) simulated star-forming galaxies at z=2 from the Millennium database. The regression they obtained between the SFR and the stellar mass of the simulated galaxies ($\log(SFR) = 0.66 \log(M_{star}) - 5.69$) gives SSFRs similar to those obtained with our model but with a steeper decrease toward high stellar masses. Finlator et al. (2006) simulated B dropouts at z=4 and also found a linear relation between the SFR and the stellar masses: $\log(SFR) = 1.14 \log(M_{star}) - 10.2$. The resulting SSFRs are slightly lower than ours at z=4, and they also exhibit a flat distribution of the SSFR with the stellar mass. The relations found by Daddi et al. (2007) and Finlator et al. (2006) are reported in Fig. 9 (panel b).

6.3.2. Redshift evolution of the metallicity

Chemical evolution models also allow predictions of the evolution of the metallicity in star-forming galaxies. While it is not the case for our sample, recent surveys have allowed to determine abundances in relatively large numbers of high redshift galaxies. We thus think it is worth presenting our models predictions for the evolution of metals.

In our models, we obtain a progressive increase in the metallicity with time, at the same tie as the stellar mass increase with more massive galaxies always being more metal-rich (as a result of the star formation histories depending on the mass). At z=0, a metallicity-stellar mass relationship is present, corresponding to the well-known luminosity-metallicity relationship (e.g. the review by Henry & Worthey, 1999).

At higher redshift, we predict that a relation still exists (see Fig. 10), but is progressively shifted to lower metallicities (by about 0.2 dex at redshift 1, 0.4 dex at redshift 2). We obtain in the models a steepening of the relationship between redshifts 1 and 0: in the more massive galaxies, the metallicity increases more rapidly because the gas reservoir is no longer replenished by primordial infall, thus the newly formed metals are less diluted even if the level of star formation is low.

We note that the obtained change in metallicity is relatively modest as the theoretical uncertainties on the models are about a factor 2 (0.3 dex, but this is a systematic effect that should not affect our trends but only shift them, as a function of both magnitude and redshift). Another uncertainty comes from the observational side: it is indeed difficult to estimate abundances, and various methods produce different results. For instance, Liang et al. (2006) have shown that the equivalent width method produces systematically higher abundances by 0.2 dex. It is thus likely that part of the difference in the observed samples discussed below is due to the method used to measure O/H. These variations in metallicity should then be addressed very carefully.

Rupke et al. (2007) have recently found that the abundances in LIRGs increased by ~0.2 dex from z~0.6 to z~0.1, which is roughly consistent with our predictions. Nevertheless, we must remain cautious since the nature of the LIRGs at low and intermediate redshift may well be different (e.g. Melbourne et al., 2005).

There are several studies of the metallicities in high redshift galaxies, or of the luminosity-metallicity relationships evolution. However, due to various selection biases and various ways of estimating the metallicities, they are often difficult to compare with each other. For this reason, no consensus has been found yet (Lamareille et al., 2006, and reference therein). In this paper, they investigated the metallicities of 131 intermediate redshift star-forming galaxies. This allowed them to compare the local and intermediate redshift (0.2 <z< 1), split in 0.2 redshift bins) mass-metallicity relationship. They did not find any significant evolution of the slope, but did find that the high redshift relationship is shifted to lower metallicities (as predicted by our model) by 0.28 to 0.55 dex (depending on the analysis performed) at z ~ 1. This is only slightly more than the value we predicted.

Savaglio et al. (2005) used the Gemini Deep Deep Survey and the Canada-France Redshift Survey to investigate the stellar mass-metallicity relationship between z ~ 0.1 and z ~ 0.7. They also found that the metallicity is lower at higher redshift for the same stellar mass by ~ 0.15 dex (according to their figure 13). They proposed a closed-box model for the chemical evolution of galaxies able to reproduce this result. This model is based on a simple exponential decline of the star formation rate after a formation redshift equal to 3. The dependence of the exponential folding time on the total mass of the galaxy is fine-tuned to reproduce the shift they found in the mass-metallicity relationship (also taking the metallicities of distant Lyman break galaxies into account). Such a model is similar in spirit to the one we propose, but ours is based on a more detailed modelization of the physics of galaxy evolution (infall, star formation law, finite lifetimes of stars) and was not fine-tuned to reproduce the evolution of a simple property between low and high redshifts but of many properties of nearby galaxies.

Hammer et al. (2005) and Liang et al. (2006) also find that $z \sim 0.7$ emission line galaxies were poorer in metals than present-day spirals, by 0.3 dex, a result also consistent with the average trend found by Maier et al. (2005). On the other hand, Kobulnicky & Kewley (2004) report a smaller variation in 0.14 dex from $z = 0$ to $z = 1$. The factor two difference with other studies might be linked to the fact that they used equivalent widths, and standard underlying stellar absorption rather than using high quality calibrated spectra and measuring the Balmer absorption. Their data suggest a steepening of the slope of the metallicity-uminosity relationship. One should also note that a direct comparison in this case is difficult since the models show the metallicity-stellar mass relationship. While luminosity scales with the mass in nearby normal galaxies, the luminosity of high redshift galaxies might be strongly affected by their current star formation rate. Going further, Erb et al. (2006) suggests that star-forming galaxies at redshift ~ 2 have 0.3 dex fainter metallicities. This is a somewhat smaller decrease than expected from our models; but taking into account the issues of selection and metallicity calibration, it is (at least) not inconsistent with them.

Because of the uncertainties in measuring metallicities and in converting stellar masses to B band luminosities, a more detailed comparison is quite pointless. We hope that Fig. 10 gives a sketch of the evolutionary trends expected in the case of secular evolution, from which eventual departures should be due to more complex physics (Rupke et al., 2007). Determinations at high redshift of star formation rates, stellar masses, and metallicities may be compared to these trends to know how much galax-

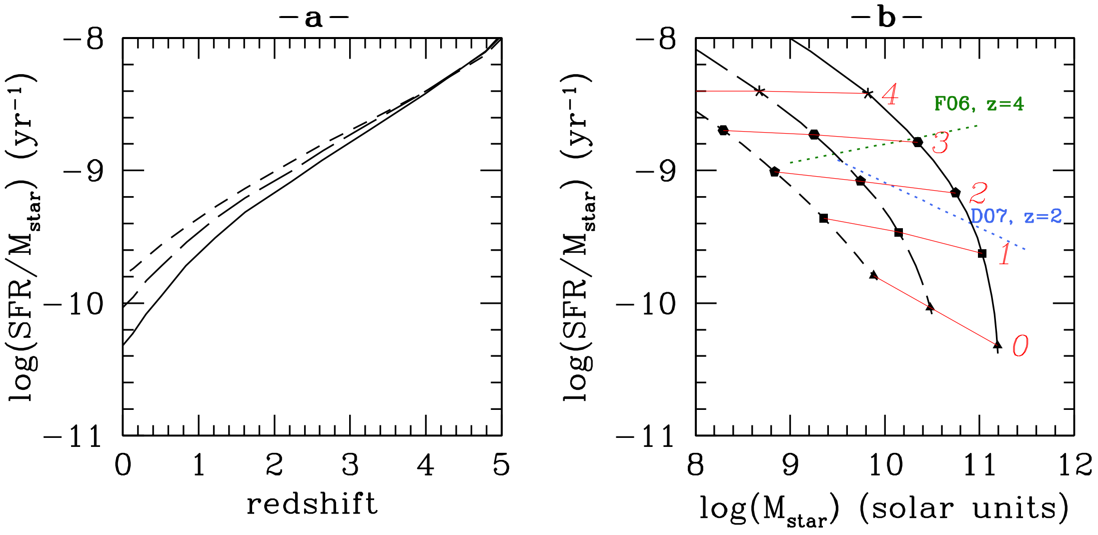

Fig. 9. Predictions of the models for higher z. All quantities are in solar units. Panel a: SSFR as a function of z for three rotational velocities and therefore masses (cf Table 1). Dotted line: 150 km s^{-1}, dashed line: 220 km s^{-1}, solid line: 360 km s^{-1}. Panel b: SSFR as a function of the stellar mass for different redshifts, each symbol corresponds to a specific redshift quoted on the plot, the values corresponding to a same redshift are connected with a red solid line. Dotted lines corresponds to the regression lines proposed for the SAMs of Finlator et al. (2006) (F06) and Daddi et al. (2007) (D07).

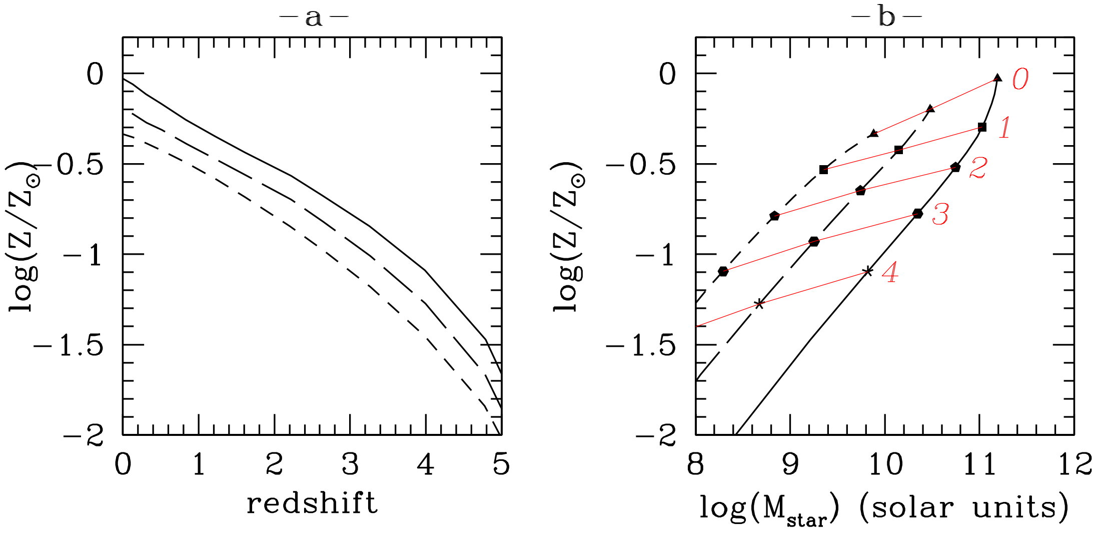

Fig. 10. Evolution of the metallicity as a function of z (panel a) and of the stellar mass (panel d), the symbols and lines are the same as in Fig. 9

ies are, on average, far from a secular evolution or not at each redshift. For instance, the values of stellar masses and metallicities in $z = 5$ Lyman break galaxies of Ando et al. (2007) are incompatible with simple secular evolution objects. It is thus likely that these objects are not precursors of normal nearby spirals.

7. Conclusions

We have analyzed the star formation rate and the stellar mass of galaxies selected to be active in star formation at z=0 and z=0.7. The selection was performed in UV and in IR (rest frame). As long as relatively massive systems are studied ($M_{\rm star} > 10^{10}\,{\rm M}_\odot$), the IR selection is found to be more efficient than the UV one to select all the star-forming systems. Nevertheless the galaxies selected in UV and in IR exhibit similar variations in the SSFR.

We compared mean relationships between the observed specific star formation rate and the stellar mass at z=0 and z=0.7 with physically motivated models aimed at reproducing the mean properties of local spiral galaxies and of the Milky Way. These models are based on a progressive infall of gas into the galactic disk starting at high z. The agreement is found to be quite good given the uncertainties in the models and the data. Both data and models exhibit a fairly flat distribution of SSFR for galaxies with masses between $10^{10}{\rm M}_\odot$ and $10^{11}{\rm M}_\odot$, this flattening being more pronounced at z=0.7 than at z=0. These results are consistent with those obtained at intermediate redshift from surveys selecting star-forming galaxies.

We have proposed an analytical formula for the mean evolution of the SFR with time and the parameters vary with the current stellar mass of the galaxy. This formulation will allow anyone to perform very simple calculations predicting e.g. star formation rates, stellar masses, or metallicities. We present predictions for the values of the specific star formation rate, stellar mass, and metallicity at high redshift. These predictions can be taken as templates for a secular evolution of galaxies, including gas accretion. They are found consistent with the mean trends deduced from the simulations of semi-analytical models up to z=4. We tentatively compared these predictions to some existing data concerning star-forming galaxies up to $z\sim2$ without finding major departures.

The comparison of model predictions with observations is difficult because of uncertainties (in observations, models, star formation rate, or metallicity calibrations) and selection biases. Thus we wish to stress that the trends presented in Fig 9 are only indications of the expected mean evolution in a simple scenario. Caution should be taken when comparing them to data. However, we believe they will still be useful for comparisons with the results of future or on going large surveys, especially if star formation rates, stellar masses, and metallicities are computed in consistent ways at different redshifts.

Acknowledgements. TTT has been supported by Program for Improvement of Research Environment for Young Researchers from Special Coordination Funds for Promoting Science and Technology commissioned by the Ministry of Education, Culture, Sports, Science and Technology (MEXT) of Japan. ELF acknowledges the support from the Spitzer Space Telescope Fellowship Program through a contract issued by JPL/Caltech and NASA. ME acknowledges the suport from the Tokyo Keizai University Research Grant (A07-05). MN was supported by the Grant-in-Aid for the Scientific Research Fund (18749007) of the Ministry of Education, Culture, Sports, Science and Technology of Japan and by a Nagasaki University president's Fund grant.

References

Ando, M., Ohta, K., Iwata at al. 2007, PASJ, 59, 717
Arnouts, Vansame, B., Benoist, C. et al. 2001, A&A, 379, 740
Baldry, I.K., Glazebrook, K., Brinkmann, J. et al. 2004, ApJ, 600, 681
Bell, E.F., McIntosh, D.H., Katz, N., & Weinberg. M.D. 2003, ApJS, 149, 289
Bell, E.F.,. 2003, ApJ, 586, 794
Bell. E.F., Wolf, C., Meisenheimer, K., et al. 2004, ApJ, 625, 23
Bell, E. F., Papovich, C., Wolf, C., et al. 2005, ApJ, 625, 23
Bell, E.F., Zheng, X.Z., Papovich, C., et al. 2007, ApJ, 663, 834
Boissier, S., Prantzos, N. 1999, MNRAS, 307, 857
Boissier, S., Prantzos, N. 2000, MNRAS, 312, 398
Boissier, S., Prantzos, N. 2001, MNRAS, 325, 321
Boissier, S., Boselli, A., Prantzos, N., & Gavazzi, G. 2001, MNRAS, 321, 733
Boissier, S., Prantzos, N., Boselli, A., & Gavazzi, G. 2003, MNRAS, 346, 1215
Boissier, S., et al. 2007, ApJS, 173, 524
Brinchmann, J., Charlot, S., White, S.D.M., et al. 2004, MNRAS, 351, 1151
Buat, V., Iglesias-Páramo, J., Seibert, M., et al. 2005, ApJ, 619, L51
Buat, V., Marcillac, D., Burgarella, D., et al. 2007, A&Ain press.
Buat, V., Takeuchi, T.T., Iglesias-Páramo, J. et al. 2007 ApJS, 173, 404
Bundy, K., Ellis, R.S., Conselice, C.J. 2005. ApJ, 625, 621
Bundy, K., Ellis, R.S., Conselice, C.J. et al. 2006. ApJ, 651, 120
Burgarella, D., et al. 2006, A&A, 450, 69
Burgarella, D., Le Floc'h, E., Takeuchi, T.T. et al. 2007, MNRAS, 380, 986
Cardelli, J. A., Clayton, G. C., & Mathis, J. S. 1989, ApJ, 345, 245
Chary, R., Elbaz, D. 2001, ApJ, 556, 562
Chary, R., Casertano, S., Dickinson, E.M. et al. 2004, ApJS, 154, 80
Chiappini, C., Matteucci, F., & Gratton, R. 1997, ApJ, 477, 765
Cooper, M.C. Newman, J.A., Weiner, B.J. et al. 2007, MNRAS, 376, 1445
Cowie, L.L., Songaila, A., Hu, E.M. & Cohen, J.G. 1996 AJ112, 839
Croton, D.J., Springel, V., White, S.D.M. et al. 2006, MNRAS, 365, 11
Daddi, E. et al. 2007, ApJ, 670, 156
Dale, D.A., Helou, G., Contursi, A., Silbermann, N.A., & Kolhatkar, S. 2001, ApJ, 549, 215
Dekel, A., Birnboim, Y. 2006, MNRAS, 368, 2
Dickinson, M. & Giavalisco, M. 2002, "The Mass of Galaxies at Low and High Redshift": ESO/US M Workshop (Venice, Italy, 24-26 October 2001), eds. R. Bender and A. Renzini. Springer-Verlag, 2003, p. 324
Elbaz, D., Daddi, E., Le Borgne, D. et al. 2007, A&A, 468, 33
Erb, D. K., Shapley, A. E., Pettini, M. et al. 2006, ApJ, 644, 813
Feulner, G., Gabash, A., Salvato, M., et al. 2005, ApJ, 633, L9
Finlator, K., Davé, R., Papovich, C., & Hernquist, L. 2006, ApJ, 639, 672
Gavazzi, G., Bonfanti, C., Sanvito, G., Boselli, A., & Scodeggio, M. 2002, ApJ, 576, 135
Goto, T., 2005, MNRAS, 360, 322
Hammer, F., Flores, H., Elbaz, D., Zheng, X. Z., Liang, Y. C., & Cesarsky, C. 2005, A&A, 430, 115
Hammer, F., Puech, M., Chemin, L., Flores, H., & Lehnert, M. D. 2007, ApJ, 662, 322
Henry, R. B. C., & Worthey, G. 1999, PASP, 111, 919
Hirashita, H., Buat, V., & Inoue, A. 2003, A&A, 410, 83
Iglesias-Páramo, Buat, V., Donas, J., Boselli, A., & Milliard, B. 2004, A&A, 419, 109
Iglesias-Páramo, Buat, V.,Takeuchi, T.T., et al. 2006, ApJS, 164, 38
Iglesias-Páramo, Buat, V., Hernandez, J. et al. 2007, ApJ, 670, 279
Kannappan, S., Gawiser, E. 2007, ApJ, 657, L5
Kitzbichler, M.G. & White, S.D.M. 2007, MNRAS, 376, 2
Kobulnicky, H. A., & Kewley, L. J. 2004, ApJ, 617, 240
Kroupa, P., Tout, C.A., Gilmore, G. 1993, MNRAS, 262, 545
Kroupa, P. 2001, MNRAS, 322, 231
Lagache, G., Dole, H., Puget, J.-L. 2003, MNRAS, 338, 555
Lamareille, F., Contini, T., Brinchmann, J., Le Borgne, J.-F., Charlot, S., & Richard, J. 2006, A&A, 448, 907
Lamareille, F. et al. 2007 in Galaxy evolution accross the Hubble time, IAU Symposium 235, 408, Cambridge University Press
Larson, R. B. 1972, Nature, 236, 7
Le Floc'h, E., Papovich, C., Dole, H., et al. 2005, ApJ, 632, 169
Liang, Y. C., Hammer, F. & Flores 2006, A&A447, 113
Leitherer, C., Schaerer, D., Goldader, J.D., et al. 1999, ApJS, 123, 3
Maier, C., Lilly, S. J., Carollo, C. M., Stockton, A., & Brodwin, M. 2005, ApJ, 634, 849
Marcillac, D., Elbaz, D., Charlot, S. et al. 2006, A&A458, 369
Martin, D. C., Small, T., Schiminovich, D. et al. 2006, ApJS, 173, 415
Melbourne, J., Koo, D. C., & Le Floc'h, E. 2005, ApJ, 632, L65
Mo, H. J., Mao, S., & White, S.D.M. 1998, MNRAS, 295, 319
Morrissey, P., Schiminovich, D., Barlow, T.A., et al. 2005, ApJ, 619, L7
Nagashima, M., Yahagi, H., Enoki, M., Yoshii, Y., & Gouda, N. 2005, ApJ, 634, 26
Noeske, K.G., Faber, S.M., Weiner, B.J. et al. 2007, ApJ, 660, L47
Pagel, B. E. J. 1997, Nucleosynthesis and Chemical Evolution of Galaxies, by Bernard E. J. Pagel. ISBN 0521550610. Cambridge, UK: Cambridge University Press.
Prantzos, N., & Boissier, S. 2000, MNRAS, 313, 338
Rupke, D. S. N., Veilleux, S., & Baker, A. J. 2007, ArXiv e-prints, 708, arXiv:0708.1766
Sandage, A. 1986, A&A, 161, 89
Sanders, D.B, Salvato, M., Aussel, H. et al. 2007, ApJS, 172, 86
Savaglio, S., et al. 2005, ApJ, 635, 260
Schaerer, D. 2007, arXiv:0706.0139
Schlegel, D. J., Finkbeiner, D. P., & Davis, M. 1998, ApJ, 500, 525
Silk, J., & Bouwens, R. 1999, After the Dark Ages: When Galaxies were Young (the Universe at $2 < Z < 5$), 470, 87
Springel, V., White, S.D.M., Jenkins, A. et al. 2005, Nature, 435, 629
Stetson, P.B. 1987, PASP, 99, 191
Takeuchi, T.T,T., Ishii, T.T., Hirashita, H. et al. 2001, PASJ, 53, 37
Takeuchi, T. T., Buat, V., Iglesias-Páramo, J., Boselli, A. & Burgarella, D. 2005a, A&A, 440. L17
Wolf, C. Bell, E. F., McIntosh, D. H., et al. 2005, ApJ, 630, 771
Wolf, C., Meisenheimer, K., Kleinheinrich, M., et al. 2004, A&A, 421, 913
Xu, C. K., Buat, V., Iglesias-Páramo, J. et al. 2006, ApJ, 646, 834
Zamojski, M.A., Schiminovich, D., Rich, R.M. et al. 2007, ApJS, in press, arXiv:astro-ph/0701478
Zheng X.Z., Bell, E.F., Papovich, C. et al. 2007, ApJ, 661, L41
Zheng X.Z., Dole, H., Bell, E.F. et al. 2007, ApJ, 670, 301